Proceedings of the ASME 2021
International Mechanical Engineering Congress and Exposition
IMECE2021
November 1-5, 2021, Virtual Conference, Online

IMECE2021-71241

PROCESS MAPPING OF ADDITIVELY-MANUFACTURED METALLIC WICKS THROUGH SURROGATE MODELING

Mohammad Borumand[1], Sima Esfandiarpour Borujeni[2], Saideep Nannapaneni[2], Moriah Ausherman[1], Guru Madiraddy[3], Michael Sealy[3], and Gisuk Hwang[1]

[1]Department of Mechanical Engineering, Wichita State University, Wichita KS 67260
[2]Department of Industrial, Systems, and Manufacturing Engineering, Wichita State University, Wichita KS 67260
[3]Department of Mechanical and Materials Engineering, University of Nebraska-Lincoln, Lincoln, NE 68588

ABSTRACT

Tailored wick structures are essential to develop efficient two-phase thermal management systems in various engineering applications, however, manufacturing a geometrically-complex wick is challenging using conventional manufacturing processes due to limited manufacturability and poor cost effectiveness. Additive manufacturing is an ideal alternative, however, the state-of-the-art metal three-dimensional printers have poor manufacturability when depositing pre-designed porous wicks with pore sizes below 100 μm. In this paper, a powder bed fusion 3D printer (Matsuura Lumex Avance-25) was employed to fabricate metallic wicks through partial sintering for pore sizes below 100 μm with data-driven control of process parameters. Hatch spacing and scan speed were selected as the two main AM process parameters to adjust. Due to the unavailability of process maps between the process parameters and properties of printed metallic wick structures, different surrogate-based models were employed to identify the combinations of the two process parameters that result in improved manufacturability of wick structures. Since the generation of training points for surrogate model training through experimentation is expensive and time-consuming, Bayesian optimization was used for sequential and intelligent selection of training points that provide maximum information gain regarding the relationships between the process parameters and the manufacturability of a 3D printed wick structure. The relationship between the required number of training points and model prediction accuracy was investigated. The AM parameters' ranges were discretized using six values of hatch spacing and seven values of scan speed, which resulted in a total of 42 combinations across the two parameters. Preliminary results conclude that 80% prediction accuracy is achievable with approximately forty training points (only 10% of total combinations). This study provides insights into the selection of optimal process parameters for the desired additively-manufactured wick structure performance.

Keywords: additive manufacturing, Bayesian optimization, laser powder bed fusion, data classification, 3D printed wick, porous materials, Gaussian, support vector machine, random forest

NOMENCLATURE

D_s	spot diameter, m
E	energy density, J/m^3
H	hatch spacing, m
P	laser power, W
U	scan speed, m/s
C	classification category
x	input variable to the classification model

Greek symbols

δ	layer thickness, m

subscripts

i	input variable

1. INTRODUCTION

Wick structures are essential parts of passive two-phase cooling systems in various applications such as high power elcotronics, spacecrafts, chemical reactors, battery, and fuel cells by enhancing spontaneous liquid coolant flow to the heated surface via wicking and increased evaporation surfaces [1,2]. A conventional manufacturing apporach such as furnace sintering has technical limitations to address growing interests in manufacturing high-performance, geometrically complex wick structures with desired pore geometries, thus it is imperative to seek a breakthrough manufacturing approach. A Laser Powder

Bed Fusion (LPBF) metal Additive Manufacturing (AM) has shown a strong potential to manufacture such complex wick structures with desired geometries and performance characteristics [3]. Recentely, Jafari et al. successfully manufactured a high-performance multi-layer wick structure with small effective pore size, 9.3 μm $< r_{eff} <$ 28.6 μm, and for a range of porosities, 2.4% $< \varepsilon <$ 42.2% by using selective sintering of the stainless steel CL 20ES particles in reduced effective laser energy [4]. They also manufactured single-layer wicks with 22 μm $< r_{eff} <$ 29 μm and 51% $< \varepsilon <$ 61% using stainless steel 316L particles [5]. To identify the required process parameters, they used trial and error based approach by carefully adjusting the laser power, scan speed, hatch spacing, fluence, layer thickness, pulse duration, and focal and point distance both in continuous and pulse lasers, mainly because the complex relations between the process parameters and wick manufacturability is still poorly understood. Furthurmore, the trial and error approach is not ideal to understand such relations due to the poor cost effectiveness, and it is imperative to seek a cost-effective approach for the process maping.

Bayesian classifer and optimization approaches are ideal candidates to fill the knowledge gap as it deals with the sequential optimal design strategy for unkonwn functions [6]. In fact, Aminzadeh and Kurfess [7] developed and trained a Bayesian classifier to detect pore generation based on the effective energy density of different sets of process parameters, but this study remains only at very low porosity below 5%, which cannot be used for the porous structures with high porosity greater than 30%, i.e., wicks.

This study examines the relation between the process parameters and additively manufactured wick manufacturability, i.e., process mapping, cost effectively by employing a surrogate-based Bayesian classifier and optimization approach. The developed approach will be also experimentally validated by the additively manufactured metallic wicks. In Section 2, we discuss the possibility of manufacturing wick structures by controlling the key process parameters in LPBF and presents the successful and failed printed wicks along with the associated process parameters. Section 3 explains the development of surrogate-based Bayesian classifier, which predicts the wick manufacturability. In Section 4, the prediction accuracy of the surrogate-based Bayesian classifier is evaluated followed by a discussion.

2. WORKING PRINCIPLES: ADDITIVELY MANUFACTURED SINTERED WICK

Figure 1 illustrates the key process parameters in LPBF metal additive manufacturing, including laser power P, hatch spacing H, scan speed U, laser spot diameter D_s, and layer thickness δ. The sintering depth and width are the thickness of the powder particles sintered in each laser pass. To manufacture desired wick structures, i.e., liquid-permeable porous structures, it requires partial-melting of the powder bed, i.e., sintering, which can be achieved by using low effective laser energy density.

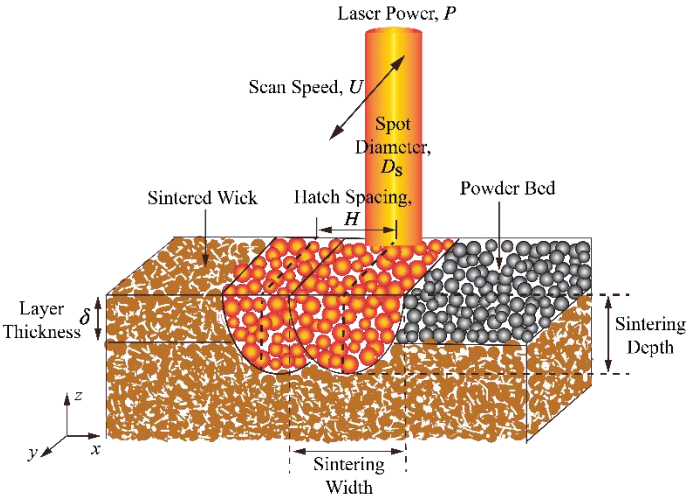

Figure 1: Schematic of powder bed fusion manufacturing process for sintered wick. Laser power, P, spot diameter, D_s, scan speed, U, hatch spacing, H, layer thickness, δ, sintering width, sintering depth, and powder bed are also shown.

The effective laser energy density E is given as [8]

$$E = \frac{P}{U \times H \times \delta} \quad (1)$$

where P is the laser power, H is the hatch spacing, and U is the scan speed, D_s is the laser spot diameter, and δ is the layer thickness. The desired low energy density can be achieved either by increasing scan speed, hatch spacing, layer thickness, spot diameter or by decreasing laser power. In this study, the layer thickness remains constant. It will be later shown that the wick manufacturability cannot be simply predicted using Eq. (1) due to complex relations between the process parameters and wick manufacturability, and the wick manufacturability will be predicted using Bayesian optimization with limited available experimental data.

3. EXPERIMENTAL: ADDITIVELY MANUFACTURED WICK

To identify the possible process parameters for additively manufactured wick structures, commercially available Stainless Steel (SS) 630 particles with powder size in the range of 20-50 μm and density of 7,750 kg/m^3 was used. The additively manufactured wick structures will be visually inspected to determine whether the wick structures are successfully manufactured or not, and the experimental results are used to train the data analytic algorithm and validate them. The SS 630 particle is an ideal choice for additive manufacturing of wick structure using partial sintering process due to good laser absorptivity and low thermal conductivity. Commercially available Matsuura LUMEX Avance-25 LFPB device which uses high-power fiber laser to selectively sinter metal particles together has been used for wick manufacturing. Before starting the print in LUMEX, the wick geometry was designed and drawn

using SolidWorks 2019 followed by defining the process parameters in the LUMEX CAM software, which were given to the Matsuura LUMEX as an input. The wick manufacturing on a build plate took about 3-4 hours. In total, 5 sets of wick structures were printed. The first 3 prints were dedicated to printing cubic wicks while prints 4 and 5 included cylindrical and strip wicks. As shown in Figure 2, a successful wick is a wick that has a consistent fully formed structure, while a failed wick denotes a wick that is structurally incoherent. If the laser effective energy density is highly low, no mechanical bond between the neighboring particles would form during the laser sintering and therefore the wick would fail.

Figure 3 shows the Scanning Electron Microscope (SEM) images of successful and failed wicks. While for a successful wick a consistent pattern of particle bond can be observed, a failed wick has inconsistent structure with hollows.

Figure 4 illustrates the manufacturability of the printed wicks as a function of their respective energy density, i.e., Eq. (1). In Figure 4, S indicates the successful wick and F represents the failed wick. The unpredictable region in Figure 4 indicates the energy densities for which no prediction can be made, using a simple predictive tool, e.g., Eq. (1). This unpredictability shows here exists a more complicated relationship between the process parameters and wick manufacturability. This is the reason why we decided to develop a statistical model for prediction of manufacturability.

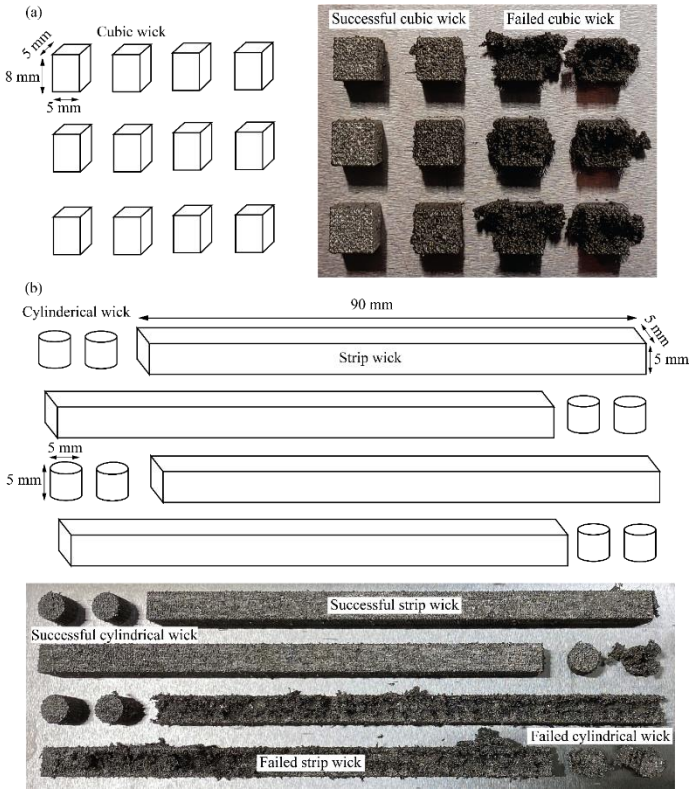

Figure 2: Schematic and pictures of successful and failed (a) cubic and (b) cylindrical and strip wicks.

4. PREDICTION OF MANUFACTURABILITY USING CLASSIFICATION METHODS

In this section, we discuss various classification to facilitate the prediction of manufacturability of a wick structure. The manufacturability is a classification problem with two outcomes (Success/Fail).

Success and Failure outcomes corresponding to the ability to manufacture the wick at a given set of process parameters. We describe five models: Naïve Bayes Classifier (NBC), Logistic Regression (LR), Support Vector Machine (SVM) Gaussian Process Classifier (GPC), and Random Forest (RF), and analyze

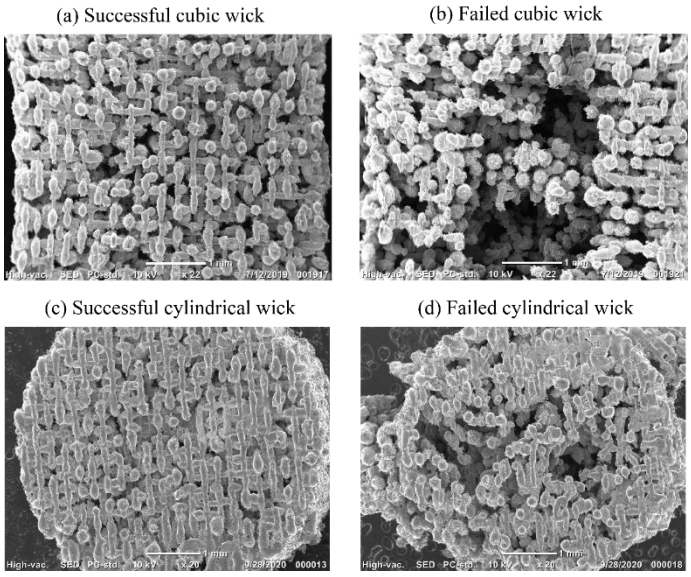

Figure 3: Scanning Electron Microscope (SEM) images of successful and failed cubic and cylindrical wicks.

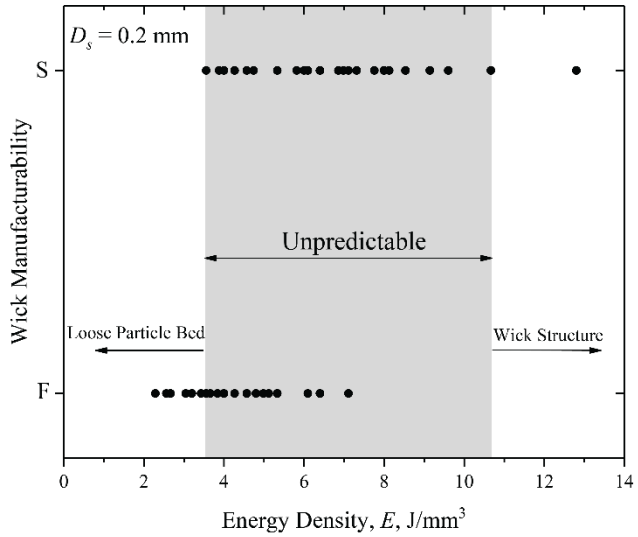

Figure 4: Wick manufacturability as a function of effective energy density at given spot diameter, D_s = 0.2 mm. The unpredictable energy density range is also shown. S and F indicate successful and failed wicks, respectively.

their abilities in manufacturability prediction. In this analysis, we considered two process parameters to predict manufacturability: scan speed, *U* (mm/s), and hatch spacing, *H* (mm). In this study, experiments are conducted at seven discrete levels of scan speed (1000, 1250, 1500, 1750, 2000, 2500, 4000 mm/s) and six levels of hatch spacing (0.2, 0.225, 0.25, 0.275, 0.3 and 0.35 mm). In general, manufacturability can also depend on other parameters such as laser power but in this preliminary study, we considered only two important parameters for this surrogate modeling study. Through this study, we try to answer the following questions:

(1) What is the prediction accuracy of these surrogate models across the input space?
(2) What is the performance of these models at the input configurations close to the boundary between successful and unsuccessful prints?
(3) What is the impact of experimental input settings on the performance of a surrogate model?

We performed 25 experiments at various input configurations to understand the manufacturability of wick structures. We use this dataset to train, validate the surrogate models and answer the above three questions. First, we will provide a brief review of the five classification models that were used in this study.

Naïve Bayes Classifier (NBC): A Naïve Bayes classifier is a probabilistic classifier in which all the input variables are assumed to be independent of each other. Let C represent the class (category) variable and let $X_i, i = 1..n$ represent n input variables. The input variables can be continuous or discrete in nature. The Naïve Bayes model uses Bayes theorem to infer the class variable given the values of the input variables. The expression for inference is given as

$$P(c|x_1, x_2 \dots x_n) = \frac{P(x_1, x_2 \dots x_n|c)P(c)}{P(x_1, x_2 \dots x_n)} = \frac{P(x_1, x_2 \dots x_n|c)P(c)}{\sum_c P(x_1, x_2 \dots x_n|c)P(c)} \quad (2)$$

Here, x_i and c represent the values taken by X_i and C respectively. $P(c)$ represents the prior probability, i.e., probability of observing class c before observing the data point $x_1, x_2 \dots x_n$. $P(x_1, x_2 \dots x_n|c)$ is the likelihood term, i.e., the probability of observing $x_1, x_2 \dots x_n$ assuming that it belongs to class c. $P(x_1, x_2 \dots x_n)$ is the probability of observing $x_1, x_2 \dots x_n$ and $P(c|x_1, x_2 \dots x_n)$ is the posterior probability of class c. Using the above expression, we calculate posterior probabilities of all values of C, and the data point $x_1, x_2 \dots x_n$ is concluded to belong to that class for which the posterior probability is the maximum.

As mentioned earlier, a Naïve Bayes classifier assumes all the input variables to be independent of each other. Using the independence property, $P(x_1, x_2 \dots x_n|c) = \prod_{i=1}^{n} P(x_i|c)$. $P(x_i|c)$ is the probability that $X_i = x_i$ given that the class is c and evaluated using its conditional distribution, which is trained using available training data. The computation of $P(x_i|c)$ depends on the type of input variable, whether discrete or continuous. Here, we detail the calculation of $P(x_i|c)$ assuming all the input variables are discrete. Let $k_i, i = 1..n$ represent the number of possible values taken by each input variable. Let $x_{ij}, i = 1..n, j = 1..k_i$ represent the j^{th}value of the i^{th} input variable. The class variable can be a binary variable of a categorical variable. We assume that C can take two values, successful and unsuccessful, denoted as 0 and 1 respectively.

$$P(x_i = x_{ij}|c) = \frac{Nijc}{N_c} \quad (3)$$

We calculate the probability that $x_i = x_{ij}$ given that the class c is calculated as the ratio of the number of data points in which $x_i = x_{ij}$ (denoted as $Nijc$) to the number of data points in the l^{th} class (denoted as N_c). The above expression is used to calculate the probabilities for all values of x_i and also, all variables $x_1, x_2 \dots x_n$. This expression is used to calculate the likelihood term, which is used in the calculation of posterior probabilities.

Support Vector Machine: Support Vector Machine (SVM) is a common machine learning algorithm, used for both regression and classification problems. The goal of SVM in classification is to find a hyperplane in a D-dimensional feature space with which all the data points could be distinctly classified [10]. The data points that are closer to the hyperplane have the main role in identifying the position and orientation of the hyperplane and are called support vectors. Support vectors are used to define a margin between the hyperplane and the data points; the goal of SVM is to maximize this margin. For binary classification, suppose that the classes are linearly separable and the discriminant function is $g(x) = w^T x + w_0$ where x had D features, w is the weights vector with D components and w_0 is a scalar. Our hyperplane-based classifier is then defined by w and w_0 and the prediction function is given by y:

$$y = Sign(w^\top x + w_0) \quad (4)$$

Now, assume that the training data set is given as $\{(x_1, r_1), \dots, (x_N, r_N)\}$, where r_n is the class label for $n \in \{1,2, \dots, N\}$, and for the hyper plane we have:

$$\begin{cases} wx^n + w_0 \geq 1 \ , r^n = +1 \\ w^n + w_0 = -1 \ , r^n = -1 \end{cases} \quad (5)$$

Equivalently,

$$r^n(w^\top x^n + w_0) \geq 1 \Rightarrow min_{1 \leq n \leq N} \mid w^\top x^n + w_0 \mid = 1 \quad (6)$$

And the hyper plane margin,ρ, will be:

$$\rho = min_{1 \leq n \leq N} \left| \frac{w^\top x^n + w_0}{\| w \|} \right| = \frac{1}{\| w \|} \quad (7)$$

Now, maximizing the margin ρ is equivalent to minimizing the norm $\| w \|$, and our optimization problem to obtain the hyperplane will be a quadratic program with N linear inequality constraints and $D + 1$ variables (w, w_0):

$$Minimize \quad f(w, w_0) = \frac{\|w\|^2}{2}$$

$$subject\ to\ \ r^n(w^\top x^n + w_0) \geq 1, \qquad n = \{1, \dots, N\}$$

This method could be extended to non-separable datasets as well. We will utilize the SVM function from the python package Scikit-learn to solve our problem.

Logistic regression: Logistic regression is a classification algorithm that can help predict a binary outcome variable. This method is often used to replicate an expert by learning from the past expert assessments. A link function (S-shaped, Sigmoidal function) is used in this method to transform the regression outcomes into a number between 0 and 1 as follows [9]:

$$p = E(Y) = \frac{\exp(\omega_0 + \omega_1 x_1 + \cdots + \omega_d x_d)}{1 + \exp(\omega_0 + \omega_1 x_1 + \cdots + \omega_d x_d)} \qquad (8)$$

which makes the $\ln(odds)$ a linear function of the predictor variable such that:

$$\ln(\text{ odds }) = \ln\left(\frac{p}{1-p}\right) = \omega_0 + \omega_1 x_1 + \cdots + \omega_d x_d \quad (9)$$

In the above equations for $i \in \{0,1,\dots d\}$, ω_i and $\hat{\omega}_i$ are the parameters and parameter estimations respectively and $E(Y)$ denotes the expectation value of the link function Y. When the predicted and fitted values match, the likelihood of an object (data point) of the dataset, i.e. $p^y(1-p)^{1-y}$ is maximized. In this method, the Log likelihood is used to estimate parameters.

Gaussian Process Classifier (GPC): Gaussian Processes (GP) are a supervised machine learning technique suitable for regression and probabilistic classification. Assume for function $f: X \to R$ we evaluated the values at n points $\{x_1, \dots, x_n\} \in X$ and form a vector $\mathbf{f}$ such that $\mathbf{f} = (f(x_1), \dots, f(x_n))$ and $\mathbf{f}$ will be a random variable. A distribution $p(f)$ is called a Gaussian process, if for any such n-dimensional subset of X, the marginal distribution over $p(f)$ has a multivariate Gaussian distribution [13]. The Gaussian Process Classifier (GCP) implements GP for classification where test predictions take the form of class probabilities. This method is based on Bayesian statistics and considers a prior distribution for the underlying probability densities while satisfying the smoothness. For binary classification a GP prior is placed over the latent function $f(x)$ and then it is squashed through the logistic logit function $\lambda(z) = (1 + exp(-z))^{-1}$ to obtain the class probability using $\pi(x) = \lambda(f(x))$. GPC is indeed a generalization of Logistic regression; Specifically, the linear function from the linear logistic model is replaced by a Gaussian process and accordingly the Gaussian prior on the weights gives its place to a GP prior [13].

Random Forest (RF): Random forests (RFs) are an ensemble learning method that can be applied to classification problems [12]. When training the RF model, one can construct a group of decision trees such that the output will be the class that appears the most among all the classes of the individual trees. Random forests are specifically useful for small data sets where the data is scarce or expensive to collect [11].

Decision Tree on the other hand, is a non-parametric method and a type of hierarchical model for supervised learning that uses a sequence of recursive split of the input space to identify local regions. A decision tree consists of internal decision nodes and terminal leaves through which a test function $f_m(x)$ would pass to label the branches [11].

An impurity measure is used to quantify the goodness of split. Assuming that N_m denotes the number of instances reaching node m and N_m^i of those instances belong to class C^i, then:

$$\hat{P}(C_i \mid \mathbf{x}, m) \equiv p_m^i = \frac{N_m^i}{N_m} \qquad (10)$$

Node m is called a pure node if for all i values, p_m^i is either 0 or 1. Otherwise, the impurity could be measured using entropy as:

$$\mathcal{I}_m = -\sum_{i=1}^{K} p_m^i \log_2 p_m^i \qquad (11)$$

In this study, the RF algorithm from Scikit-learn is utilized for classification.

5. RESULTS AND DISCUSSION

5.1 Additively Manufactured Wicks

In this section, the effect of the process parameters on wick manufacturability is discussed based on the experimental results, i.e., additively-manufactured wicks using LPBF. The process parameters were initially selected by following a trial-and-error approach that was based on the idea of achieving partial sintering through careful reduction of the effective laser energy density, Based on Eq. (1), energy density is directly proportional to laser power, P, and inversely proportional to hatch spacing, H, scan speed, U, and layer thickness, δ. However, Eq. (1) provides no information regarding the possible effect of the spot diameter, D_s, on laser energy density. Therefore, the sets of process parameters that are known to generate minimal pores, i.e., H = 0.15 mm, U = 700 mm/s, P = 320 W, D_s = 0.2 mm, and δ = 0.02 mm, were adjusted with the aim of reducing the energy density. These set of parameters were provided by the Lumex Corporation catalogue. The following process parameters were employed to additively manufacture wicks: spot diameter and layer thickness were fixed at D_s = 0.2 mm and δ = 0.02 mm, respectively, and two values for laser power, P = 120 and 160 W, six different values for hatch spacing, H = 0.2, 0.225, 0.25, 0.275, 0.3, and 0.35 mm (0.2 mm ≤ H < 0.35 mm), and seven values for scan speed, U = 1000, 1250, 1500, 1750, 2000, 2500, and 4000 mm/s (1000 mm/s ≤ U < 4000 mm/s) were selected.

After printing the wick structures, it was found that the selected laser power range, i.e., 120 W ≤ P ≤ 160 W, was not broad enough to capture laser sensitivity to wick manufacturability.

Figure 5 illustrates wick manufacturability as a function of hatch spacing and scan speed at D_s = 0.2 mm and 120 W ≤ P ≤ 160 W. It can be seen that variations of scan speed and hatch spacing have huge impacts on wick manufacturability. More specifically, while selecting extremely low hatch spacings and scan speeds would significantly increase the possibility of wick manufacturability (due to the increased energy density),

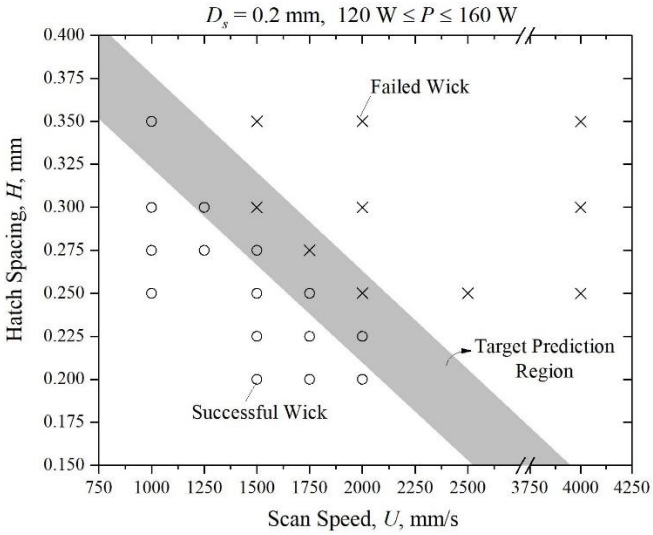

Figure 5. Wick manufacturability as a function of hatch spacing, H, and scan speed, U, at given spot diameter, D_s = 0.2 mm and laser power, 120 W ≤ P ≤ 160 W.

increasing these two parameters above a certain threshold range, which is shown by the Target Prediction Region in Figure 5 results in structurally inconsistent wick, i.e., failed wick structures. This is the region that is critical to predict using Bayesian approach, which will be explained in detail in the next sections.

Table **1** summarizes the process parameters and wick manufacturability associated with the data shown in Figure 5.

Table 1. Process parameters associated with successful and failed additively-manufactured wicks at spot diameter D_s = 0.2 mm.

Print #	Hatch Spacing, H, mm	Scan Speed, U, mm/s	Laser Power, P, W	Successful Print?
1	0.2	1500	120	O
2	0.2	1750	120	O
3	0.2	1750	160	O
4	0.2	2000	120	O
5	0.2	2000	160	O
6	0.225	1500	120	O
7	0.225	1750	120	O
8	0.225	1750	160	O
9	0.25	1000	100	O
10	0.25	1000	160	O
11	0.25	1500	100	O
12	0.25	1500	120	O
13	0.25	1500	160	O
14	0.25	1750	160	O
15	0.275	1250	120	O
16	0.275	1500	120	O
17	0.275	1500	160	O
18	0.3	1000	120	O
19	0.3	1000	160	O
20	0.35	1000	160	O
21	0.25	2000	100	X
22	0.25	2000	120	X
23	0.25	2000	160	X
24	0.25	2500	100	X
25	0.25	2500	120	X
26	0.25	2500	160	X
27	0.25	4000	160	X
28	0.275	1750	120	X
29	0.3	1250	120	X
30	0.3	1500	120	X
31	0.3	1500	160	X
32	0.3	2000	120	X
33	0.3	2000	160	X
34	0.3	4000	160	X
35	0.35	1500	120	X
36	0.35	1500	160	X
37	0.35	2000	120	X
38	0.35	2000	160	X
39	0.35	4000	160	X

5.2 Surrogate modeling

Simulation study: First, we considered three different train/test proportions of the dataset: 60/40, 70/30, 80/20. In the dataset of 25 points, 15 points correspond to successful prints and 10 correspond to failed prints. From Figure 5, there are five success points and three failure points in the target region. To create balanced datasets for training the classifiers, we assumed similar proportion of success and failure data points. Since prediction in the target region is crucial, we added four points (two success and two failure) to the training dataset. Table 2 shows the total number of data points used for training and testing at three different train/test splits. For 60/40 proportion, we used 15 data points for training and 10 for testing. We considered 8 success points and 7 failure points in those 15 points used for training. Out of 8 success points, 2 success points were chosen from the target region. Similarly, 2 failure points were chosen from the target region and 5 points were chosen away from the target points. Table 3 shows the proportion of success training and testing points from the target and away from target regions across various train/test splits. Similarly, table 4 shows the proportion of failure training and testing points from the target and away from target regions across various train/test splits.

Table 2. Total number of training and testing points in various train/test splits

	Train/Test split		
	60/40	70/30	80/20
Number of train data points	15	18	20
Number of test data points	10	7	5

Table 3. Number of success points (boundary and other) used in various train/test splits

	Train/Test split		
	60/40	70/30	80/20
Total Success Points	15	15	15
Total Success Points (Training)	8	9	11
Total Success Points (Testing)	7	6	4
Total Success Points (Training)	8	9	11
Success Points (Boundary)	2	2	2
Success Points (Other)	6	7	9
Total Success Points (Testing)	7	6	4
Success Points (Boundary)	3	3	3
Success Points (Other)	4	3	1

Table 4. Number of failure points (boundary and other) used in various train/test splits

	Train/Test split		
	60/40	70/30	80/20
Total Failure Points	10	10	10
Total Failure Points (Training)	7	8	9
Total Failure Points (Testing)	3	2	1
Total Failure Points (Training)	7	8	9
Failure points (Boundary)	2	2	2
Failure Points (Other)	5	6	7
Total Failure Points (Testing)	3	2	1
Failure points (Boundary)	1	1	1
Failure points (Other)	2	1	0

We used the same set of success/failure training points from the target region across various train/test splits. For 70/30 split, we used all the training points used in 60/40 split and added three more points away from the target region. Similarly, we used all the points in 70/30 split and added a couple more training points to obtain the 80/20 split dataset. Using the data sets with various train/test splits, we estimated the prediction performance of various classifiers built with the same training dataset, at the test points and specifically the points in the target region. As mentioned above, there are 5 success and 3 failure points in the target region, and 2 success and 2 failure points are used in the training dataset. Therefore, we performed the prediction at the remaining 3 success and 1 failure points. For the 60/40 split, there are a total of 10 test points. Since four of them are in the target region, the remaining six are away from the target region. In the case of 80/20 split, there are a total of 5 test points with four of them in the target region. To obtain the uncertainty in the prediction performance, we repeated the analysis 10 times choosing the training and testing data points at random. Figure 6 shows the box plots of prediction accuracy of the five classifiers across the three train/test splits at the test data points.

Figure 6 shows the overall prediction accuracy; this contains predictions at test points in and away from the target region. Figure 7 shows the box plots of the prediction accuracy of the five classifiers across various train/test splits at the test points in the target region. There is a total of 4 test points (3 success and 1 failure) in the target region.

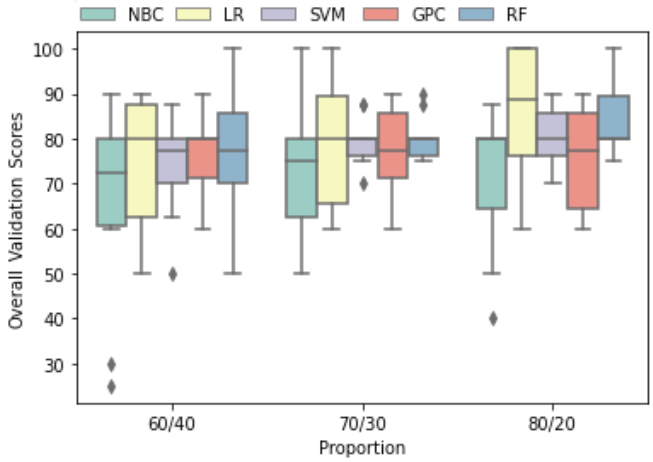

Figure 6. Prediction accuracy of the five classifiers across various train/test split proportions.

We can make the following observations from Figures 6 and 7. The overall prediction accuracy increases slightly for most models (LR, SVM, RF) while the performance remains the same at the other two models (NBC, GPC). According to Figure 7, there is a slight improvement in the prediction accuracy in the target region with the train/test split proportion. At 80/20 split, there is some evidence that the prediction accuracy reaches 100% for all the five models whereas the prediction accuracy reached 100% for one model and two models for 60/40 and 70/30 splits respectively. The reason for not observing a significant change in the prediction accuracy is because the additional training points added in the 80/20 split when compared to the 60/40 split were away from the target region and therefore had little impact in the prediction accuracy in the target region.

Next, we perform an empirical analysis to test if the prediction performance increases in the target region when more points from the target region are added to the training dataset. For this study, we considered 60/40 split, which contains 15 training and 10 testing data points.

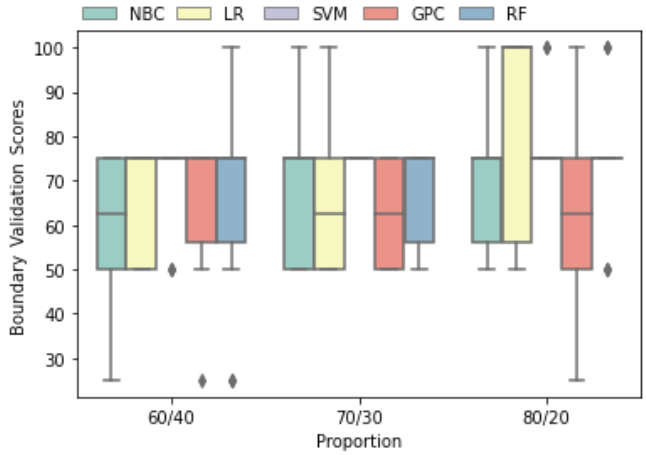

Figure 7. Prediction accuracy of the five classifiers across various train/test split proportions in the target region.

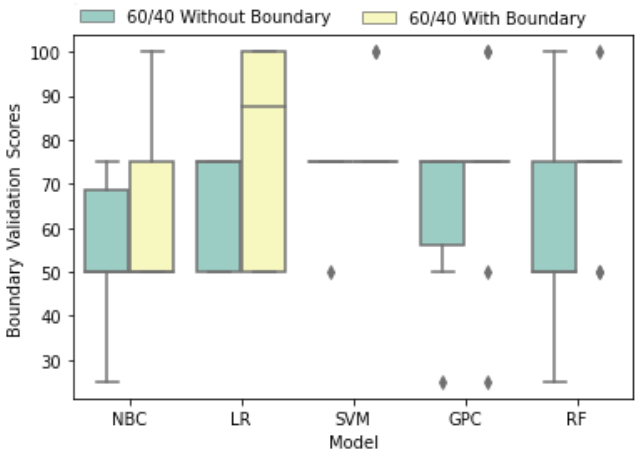

Figure 8. Prediction accuracy of the five classifiers in the target region with and without considering training points from the target region.

In the above analysis, we considered four points from the target region in the training dataset. Now we repeated the analysis considering all the data points in the training dataset away from the target region. In one case, we considered 15 training data (8 success and 7 failure) with 4 points (2 success and 2 failure) from the target region while the remaining 11 points (6 success and 5 failure) are selected away from the target region. In the other case, all the 15 training data (8 success and 7 failure) are selected away from the target region. We trained all the five classifiers at both these cases and predicted their prediction performance at the four remaining points (3 success and 1 failure) in the target region. We repeated the analysis 10 times with random selection of training data points. Figure 8 shows the boxplots compares the prediction performance in the two cases across the five models.

Figure 8 shows that the prediction performance of models trained with training points from the target region is slightly higher than those models trained without points from the target region. The prediction performance of all the five models reach 100% when points from the target region are considered. From Figures 6-8, the random forest model provides better overall and boundary prediction performance.

6. CONCLUSION

In this paper, we studied a surrogate-based approach to predict manufacturability of an additively manufactured metallic wick structure using two process parameters: scan speed and hatch spacing. Here, we investigated the performance of five different classifiers: Naïve Bayes Classifier, Logistic Regression, Support Vector Machine, Gaussian Process Regression and Random Forest. We studied the effect of the training and testing data proportion on the prediction performance across the input parameter space and close the boundary between successful and unsuccessful prints. This paper also investigated the effect the training point selection on the prediction performance of the surrogate model performance. The surrogate prediction results were compared with experiments.

As a future work, we will consider an experimental design framework to intelligently and adaptively choose the process parameters that provide maximum information to the surrogate model in approximately the experimental results. In addition, we will also investigate the estimation of optimal process parameters that optimize the wick performance (e.g., porosity).

ACKNOWLEDGEMENT

This work is financially supported by the National Science Foundation (NSF), Award No. OIA-1929187 and the Wichita State University Convergence Sciences Initiative Program. This work is also financially supported by the College of Engineering, Wichita State University.

REFERENCES

[1] Faghri, A., 1995, *Heat Pipe Science And Technology*, Taylor & Francis.

[2] Liter, S. G., and Kaviany, M., 2001, "Pool-Boiling CHF Enhancement by Modulated Porous-Layer Coating: Theory and Experiment," Int. J. Heat Mass Transf., **44**(22), pp. 4287–4311.

[3] Jafari, D., Wits, W. W., and Geurts, B. J., 2018, "Metal 3D-Printed Wick Structures for Heat Pipe Application: Capillary Performance Analysis," Appl. Therm. Eng., **143**, pp. 403–414.

[4] Jafari, D., Wits, W. W., Vaneker, T. H. J., Demir, A. G., Previtali, B., Geurts, B. J., and Gibson, I., 2020, "Pulsed Mode Selective Laser Melting of Porous Structures: Structural and Thermophysical Characterization," Addit. Manuf., **35**, p. 101263.

[5] Jafari, D., van Alphen, K. J. H., Geurts, B. J., Wits, W. W., Gonzalez, L. C., Vaneker, T. H. J., Rahman, N. U., Römer, G. W., and Gibson, I., 2020, "Porous Materials Additively Manufactured at Low Energy: Single-Layer Manufacturing and Characterization," Mater. Des., **191**, p. 108654.

[6] Smith, R. C., 2013, *Uncertainty Quantification: Theory, Implementation, and Applications*, SIAM.

[7] Aminzadeh, M., and Kurfess, T. R., 2019, "Online Quality Inspection Using Bayesian Classification in Powder-Bed Additive Manufacturing from High-Resolution Visual Camera Images," J. Intell. Manuf., **30**(6), pp. 2505–2523.

[8] Gong, H., Rafi, K., Gu, H., Starr, T., and Stucker, B., 2014, "Analysis of Defect Generation in Ti–6Al–4V Parts Made Using Powder Bed Fusion Additive Manufacturing Processes," Addit. Manuf., **1–4**, pp. 87–98.

[9] Foreman, J. W., Jennings, G., & Miller, E. (2014). Data smart: Using data science to transform information into insight (Vol. 1). Indianapolis: Wiley.

[10] Wang, L. (Ed.). (2005). Support vector machines: theory and applications (Vol. 177). Springer Science & Business Media.

[11] Alpaydin, E. (2020). Introduction to machine learning. MIT press.

[12] Ho, T. K. (1998). The random subspace method for constructing decision forests. IEEE transactions on pattern analysis and machine intelligence, 20(8), 832-844.

[13] Rasmussen, C. E. (2003, February). Gaussian processes in machine learning. In Summer school on machine learning (pp. 63-71). Springer, Berlin, Heidelberg.